IEEE Access
Multidisciplinary ⋮ Rapid Review ⋮ Open Access Journal

Received April 24, 2020, accepted May 11, 2020, date of publication May 14, 2020, date of current version June 1, 2020.

Digital Object Identifier 10.1109/ACCESS.2020.2994625

Experimental Study of High Performance 4H-SiC Floating Junction JBS Diodes

HAO YUAN[1], CHENGSEN WANG[2], XIAOYAN TANG[1], QINGWEN SONG[1], YANJING HE[1], YIMEN ZHANG[1], (Senior Member, IEEE), YUMING ZHANG[1], (Senior Member, IEEE), LI XIAO[3], LIANGYONG WANG[3], AND YONG WU[4]

[1]School of Microelectronics, Xidian University, Xi'an 710071, China
[2]Jie Jie Semiconductor Company, Ltd., Nantong 226200, China
[3]ZTE Corporation, Shenzhen 518063, China
[4]Xidian-Wuhu Research Institute, Wuhu 241000, China

Corresponding authors: Xiaoyan Tang (xytang@mail.xidian.edu.cn) and Qingwen Song (qwsong@xidian.edu.cn)

This work was supported in part by the National Natural Science Foundation of China under Grant 61804118, Grant 61774117 and Grant 61774119, in part by the Key Research and Development Program of Shaanxi under Grant 2020ZDLGY03-07, in part by the Shaanxi Science & Technology Nova Program under Grant 2019KJXX-029, in part by the Innovation platform construction project of 2018 Wuhu Science and Technology Plan under Grant 2018pt02, in part by Wuhu and Xidian University special fund for industry-university-research cooperation under Grant XWYCXY-012019001, and in part by the Fundamental Research Funds for the Central Universities under Grant 20106205935.

ABSTRACT This paper reports the demonstration of a high performance 4H-SiC floating junction junction barrier Schottky (FJ_JBS) rectifier with a 30μm, 6×10^{15} cm^{-3}-doped epitaxial layer. Extensive simulations have been performed to design, optimize and analyze the structure of the FJ_JBS rectifier. The fabricated FJ_JBS shows that breakdown voltage (BV) and differential $R_{on,sp}$ are 3.4 kV, yielding the highest BV value reported for 4H-SiC FJ diodes, and 5.67 m$\Omega\cdot$cm^2, respectively. Compared with the conventional JBS, the BV value of FJ_JBS increases by 33.3% and the $R_{on,sp}$ only slightly rises by 6.2%. The corresponding Baliga figure-of-merit (BFOM) ($4\ BV^2/R_{on-sp}$) of this FJ_JBS diode is 8.16 GW/cm^2.

INDEX TERMS 4H-SiC, FJ structure, JTE termination, FJ_JBS.

I. INTRODUCTION

4H-SiC power devices have received much attention for high-power applications due to the outstanding properties of this material, including its large critical electric field and high thermal conductivity [1]. Junction barrier Schottky (JBS) diodes, which were the first commercialized SiC devices, are ideal device for medium-voltage and fast-switching applications [2], [3]. However, there is a tradeoff between the breakdown voltage (BV) and specific on-resistance (R_{on-sp}) for conventional JBS structure, constraining further improvements to device performance. To solve this issue, the floating junction (FJ) structure has been applied to 4H-SiC power devices [4], [5]. This new structure can modulate the electric field distribution in the drift region, greatly improving BV at a constant R_{on-sp}. However, although the shape of the FJ structure, design of the FJ structure underneath the termination region have been analyzed and reported, the design of the FJ device is still complex because the epitaxial layer parameters and the work mechanism of the termination structure should be redesigned and reanalyzed [6]–[9].

In this paper, the design of the epitaxial layer and termination structure for the FJ_JBS structure are first described and analyzed. Then, based on the analysis, we report the fabrication and experimental study of a high-performance 4H-SiC FJ_JBS rectifier adopting the designed epitaxial layer and termination structure. Finally, the conventional device and the FJ device are compared in terms of performance.

The associate editor coordinating the review of this manuscript and approving it for publication was Alexander Micallef.

II. DEVICE STRUCTURE ANALYSIS

A. FJ_JBS DEVICE STRUCTURE

The structures and electric field distributions at the breakdown condition of the conventional JBS and FJ_JBS are shown in Figure 1. For the conventional structure, it is clear that the depletion layer in the epitaxial layer extends from the surface to the substrate as the reverse voltage increases. There are three cases for the electric field distribution dependent on the doping concentration of the epitaxial layer (N_D) (assuming that the thickness of the epitaxial layer is constant), as shown in Figure 1(a).

This work is licensed under a Creative Commons Attribution 4.0 License. For more information, see https://creativecommons.org/licenses/by/4.0/

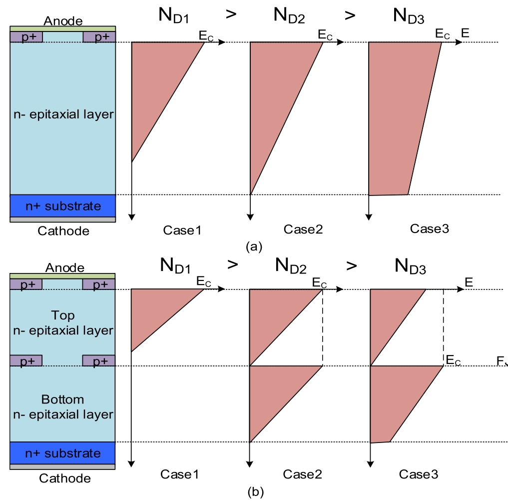

FIGURE 1. **Structures and electric field distributions at the breakdown condition of the (a) conventional JBS, and (b) FJ_JBS.**

1) Case 1 (Non-punch-through state): When N_D is at N_{D1}, the electric field at the surface reaches the critical value before the depletion layer extends to the substrate, producing a single triangular electric field distribution in the epitaxial layer.
2) Case 2 (Critical state): With N_D decreasing ($N_{D2} < N_{D1}$), if the electric field at the surface reaches the critical value when the depletion layer extends just to the substrate, then there is also a single triangular electric field distribution in the epitaxial layer.
3) Case 3 (Punch-through state): When N_D is at N_{D3}($N_{D3} < N_{D2}$), the electric field at the surface reaches the critical value after the depletion layer extends to the substrate, implying there is a trapezoidal electric field distribution or even a rectangular electric field distribution when N_D is too light in the epitaxial layer at the breakdown condition.

For the *FJ* device, because the FJ structures (p+ region) in the FJ device are discrete and floating, there is no potential difference between the FJ structure and surrounding epitaxial layer at the zero bias, indicating that the space between the two adjacent FJ structures is not pinched off by the depletion area and that there is a current path between the two adjacent FJ structures. Under this condition, the FJ device can be seen as a single pn junction between the top p+ area and the whole epitaxial layer. Therefore, when the lower reverse voltage is applied to the device, the depletion layer occurs only in the top epitaxial layer (extending form the surface to the FJ structure), which is consistent with the conventional device. With the reverse voltage increasing, the boundary of the depletion layer in the top epitaxial layer extends to the FJ structure. The depletion area in the top epitaxial layer is terminated at the FJ structure, showing a p^+-n^--p^+ punched-through structure and the pn junction between the FJ structure and top epitaxial layer is forward bias. The forward biased pn junction makes that the electric field at the top boundary of the FJ structure should be nearly zero, inferring that the electric field distribution in the top epitaxial layer is nearly unchanged and triangular and that the voltage drop in the top epitaxial layer remains nearly unchanged too. Therefore, with the reverse voltage increasing continually, the pn junction between the FJ and bottom epi-layer is reversed and then the voltage-drop of the bottom epitaxial layer rises. At the same time, the space between the two FJ structures is completely pinched off, and the peak electric field at the surface may remain nearly unchanged, indicating that the breakdown occurs at the FJ structure instead of the surface with the reverse voltage increasing continually. Therefore, it is known that the depletion layer in the epitaxial layer first extends from the surface to the *FJ* structure with the reverse voltage rising. Combined with our previous work [10], there are also three cases for the electric field distribution with different N_D values (assuming that the thickness of the epitaxial layer is constant and the FJ structure is located in the middle of the epitaxial layer), as shown in Figure 1(b).

1) Case 1 (Premature breakdown state): When N_D is at N_{D1}, which is larger than N_{D1} in the Case 1 (top), the peak electric field at the surface reaches the critical value before the depletion layer extends to the *FJ* structure and the space between the *FJ* structure is pinched off by the depletion layer, implying premature breakdown occurs at the surface. There is only one triangular electric field distribution in the top epitaxial layer.
2) Case 2 (Critical state): With N_D decreasing ($N_{D2} < N_{D1}$), if the peak electric field (which is infinitely close to the critical value) at the surface does not reach the critical value when the depletion layer extends to the *FJ* structure and the space between the *FJ* structure is pinched off by the depletion layer, the triangular electrical field distribution in the top epitaxial layer remains nearly unchanged, and the depletion layer extends from the *FJ* structure to the substrate with the reverse voltage increasing continually. Under this condition, breakdown occurs at the *FJ* structure, which improves the reverse performance of the *FJ* device. Because the thicknesses of the top and bottom epitaxial layers are the same and the peak electric field at the surface is infinitely close to the critical value, the peak electric field at the *FJ* structure reaches the critical value when the depletion layer extends just to the substrate at the breakdown condition, indicating that the electric field distributions at the top and bottom are nearly the same, shown as two triangular shapes.
3) Case 3 (Punch-through state): When $N_{D3} < N_{D2}$, the electric field distribution at the top is triangular but the peak electric field at the surface is lower than the critical value. Under this condition, the peak electric field at the *FJ* structure reaches the critical value first, and the electric field distribution at the bottom

is trapezoidal or even rectangular at the breakdown condition, which is different from the electric field distribution at the top.

Therefore, the electric field distribution can be divided into two parts when the *FJ* structure works normally, where the slope of each electric field distribution is higher than that of the conventional structure. Compared to the conventional device, the epitaxial layer resistance decreases in the *FJ* device because a higher N_D value is adopted to increase the slope of the electric field distribution at the same epitaxial layer thickness. Thus, it can be concluded that there is a new tradeoff between *BV* and R_{on-sp} for the *FJ* device and that the epitaxial layer should be redesigned to improve the performance of the *FJ* device over that of the conventional device.

B. DESIGN OF THE EPITAXIAL LAYER FOR THE FJ_JBS

According to the analysis above, the parameters of the epitaxial layer for the *FJ* devices should first be designed. Typically, an epitaxial layer thickness of 30 μm is used for a 3 kV-rating SiC device. Therefore, the thickness of the epitaxial layer is selected as 30 μm, and N_D should be redesigned for the *FJ* device. Based on our previous work [10], Figure 2(a), (b) and (c) show R_{on-sp}, *BV* and Baliga figure-of-merit (BFOM) of the FJ_JBS and conventional JBS for comparison versus N_D, where the *FJ* structure is located in the middle of the epitaxial layer and the thickness, width and spacing of the *FJ* structure are 0.8 μm, 3 μm and 3 μm, respectively. Figure 2(a) shows that the R_{on-sp} of the *FJ* device decreases with increasing N_D, which is consistent with the behavior of the conventional structure.

However, it is obvious that there is a very large difference in the *BV* distribution between the *FJ* and conventional device structures, as shown in Figure 2(b). *BV* exhibits an inflection point when N_D is approximately 7.5×10^{15} cm^{-3}. According to the working mechanism of the *FJ* device described above, it can be concluded that 7.5×10^{15}cm^{-3} is a critical value (Case 2: Critical state). If N_D is lower than the inflection point in our analysis, the electric field distribution corresponds to Case 3: Punch-through state. The depletion layer can extend to the *FJ* structure successfully before the electric field at the surface reaches the critical value, implying that the electric field distribution appears in both the top and bottom of the epitaxial layers. Otherwise, premature breakdown occurs at the surface, indicating that the *FJ* structure does not work (Case 1: Premature breakdown state).

Moreover, to improve the tradeoff between *BV* and R_{on-sp}, BFOM ($4BV^2/R_{on-sp}$) versus N_D is displayed in Figure 2(c) to help design N_D appropriately. The BFOM of the *FJ* device also has an inflection point induced by the *BV* distribution. The BFOM first increases with increasing N_D and drops sharply when N_D exceeds the inflection point. Thus, N_D should be lower and closer to the inflection point to achieve better performance. Our analysis suggests that the doping concentration window of the *FJ* device is between

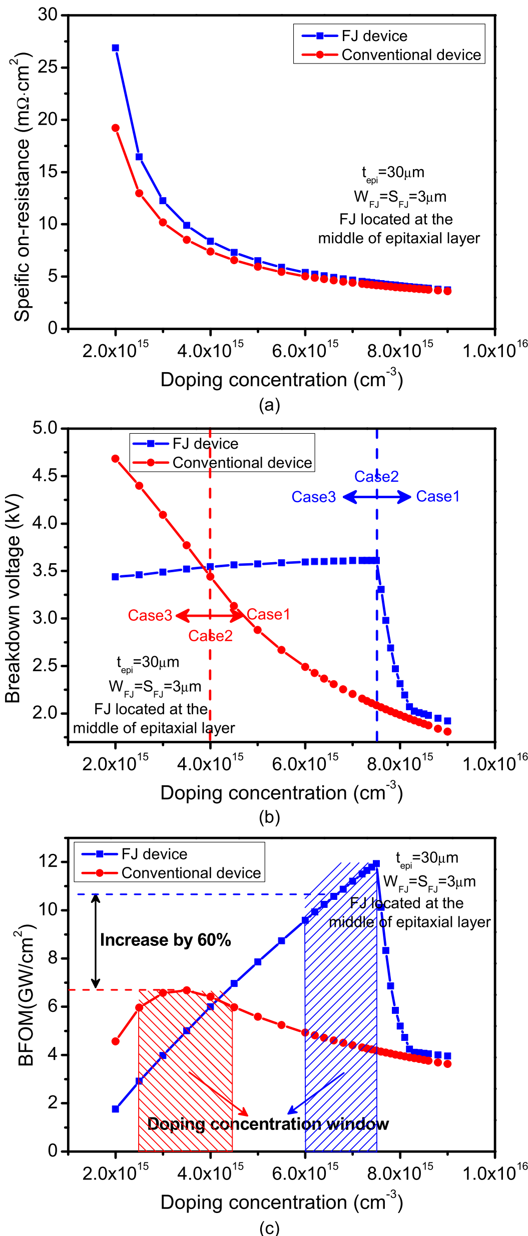

FIGURE 2. Dependence of R_{on-sp} (a) BV (b) and BFOM (c) in FJ device and conventional device for varying N_D.

6×10^{15}cm^{-3} and 7.5×10^{15} cm^{-3}, which is different from the configuration of the conventional device. Moreover, the BFOM of the *FJ* device can be increased by approximately 60% compared with the conventional device configuration at suitable N_D when the thickness of the epitaxial layer is constant, implying that the *FJ* device performs better. Considering the deviation in the epitaxial layer parameters and termination efficiency, the doping concentration and thickness of the epitaxial layer for the *FJ* device are selected as 6×10^{15} cm^{-3} and 30 μm in our work, respectively, where the *FJ* structure is located in the middle of the epitaxial layer. The parameters of the epitaxial layer designed for the *FJ* device are shown in Table 1 too, and the optimal values of R_{on-sp} and

TABLE 1. Parameters of the epitaxial layer.

Parameters	*Value*
Doping concentration	6×10^{15} cm^{-3}
Total thickness	30 μm
Thickness of the bottom layer	15 μm
Thickness of the top layer	15 μm
FJ width	3 μm
FJ spacing	3 μm

BV are 5.4 mΩ·cm^2 and 3.6 kV, respectively, corresponding to a BFOM of 9.6 GW/cm^2.

C. MODELS AND PARAMETERS USED IN THE SIMULATIONS

To achieve precise results, the simulations are carried out using the 2-D device simulator ISE-DESSIS at room temperature. The primary function of this simulator is to solve Poisson's equation along with the continuity and drift diffusion equations to simulate the characteristics of a semiconductor device. The most important simulation models, such as the incomplete ionization model, carrier generation-recombination model and impact ionization model, are used in our analysis without considering dopant activation or defects.

1) INCOMPLETE IONIZATION MODEL

Because of the large ionization energies, the dopants in 4H-SiC are actually in the freeze-out regime at room temperature. Therefore, incomplete ionization should be considered, as shown below [11], [12]:

$$N_A^+ = N_A\left[\frac{\left(1+4g_A\left(\frac{N_A}{N_V}\right)e^{\frac{E_A}{kT}}\right)^{0.5}-1}{2g_A\left(\frac{N_A}{N_V}\right)e^{\frac{E_A}{kT}}}\right] \quad (1)$$

$$N_D^+ = N_D\left[\frac{\left(1+4g_D\left(\frac{N_D}{N_C}\right)e^{\frac{E_D}{kT}}\right)^{0.5}-1}{2g_D\left(\frac{N_D}{N_C}\right)e^{\frac{E_D}{kT}}}\right] \quad (2)$$

where N_D and NA are the total doping concentrations and EA and ED are the acceptor and donor ionization energy levels, respectively (EA (Al)≈200 meV, ED(N)≈90 meV) [13]. In addition, k_B is the Boltzmann constant, and g_A and g_D are the appropriate degeneracy factors for the valence and conduction bands, which are assumed to be 4 and 2, respectively. Moreover, N_V and N_C are the densities of states for holes and electrons, respectively, which can be described as [14]

$$N_V = 2.494\times10^{19}\cdot\left(\frac{T}{300}\right)^{3/2} \quad (3)$$

$$N_C = 1.689\times10^{19}\cdot\left(\frac{T}{300}\right)^{3/2} \quad (4)$$

Carrier Generation-Recombination Model: The Shockley-Read-Hall (SRH) and Auger recombination models are used in this work to simulate the carrier generation-recombination effect. The SRH recombination-generation rate and Auger recombination rate are modeled with the equations below [13], [15]–[17]:

$$R_{SRH} = \frac{pn-n_i^2}{\tau_{p0}\left[n+n_i\exp\left(\frac{E_t-E_i}{kT}\right)\right]+\tau_{n0}\left[p+n_i\exp\left(\frac{-E_t-E_i}{kT}\right)\right]} \quad (5)$$

$$R_{Auger} = 3\times10^{-29}\left(pn^2-nn_i^2\right)+3\times10^{-29}\left(np^2-pn_i^2\right) \quad (6)$$

Here, n_i is the effective intrinsic carrier concentration, Ei is the intrinsic Fermi level, and Et is the recombination center energy level, which is set to 0 in our simulation. Moreover, $\tau n0$ and $\tau p0$ are the electron and hole lifetimes, which are assumed to be 2.5 μs and 0.5 μs, respectively.

2) IMPACT IONIZATION MODEL

The carrier generation rate in the avalanche breakdown condition is described by the equation below:

$$G = \alpha_n J_n + \alpha_p J_p \quad (7)$$

where αn and αp are the impact ionization coefficients for electrons and holes, and Jn and Jp are the electron and hole current densities, respectively. The impact ionization coefficients are modeled as:

$$\alpha_{n,p} = A_{n,p}\exp\left[\left(\frac{B_{n,p}}{E}\right)^{C_{n,p}}\right] \quad (8)$$

where E is the electric field in the direction of current flow. $A_{n,p}$, $B_{n,p}$ and $C_{n,p}$ are respectively found to be 7.26×10^6cm, 2.34×10^7V/cm and 1 for electrons, and 6.85×10^6cm, 1.41×10^7V/cm and 1 for holes by fitting the reported experimental results [18], [19].

D. DESIGN AND ANALYSIS OF THE TERMINATION STRUCTURE FOR THE FJ_JBS

In addition, a junction termination extension (JTE) structure is designed for the *FJ* device to achieve excellent reverse performance. The schematic cross-section of the FJ_JBS diode with the optimized termination structure is shown in Figure 3(a). According to our previous work [9], the FJ structure underneath the termination region is selected as the discontinuous floating junction structure in this work to protect the FJ structure underneath the termination region from occurring premature breakdown.

Here, a guard-ring-assisted JTE plus outer-rings (GA-JTE-OR) structure is adopted for our designed *FJ* device [20]. This choice mainly arises from two aspects. 1) Compared with double-zone JTE, step-double-zone-JTE and counter-doped JTE, the fabrication process of GA-JTE-OR is compatible

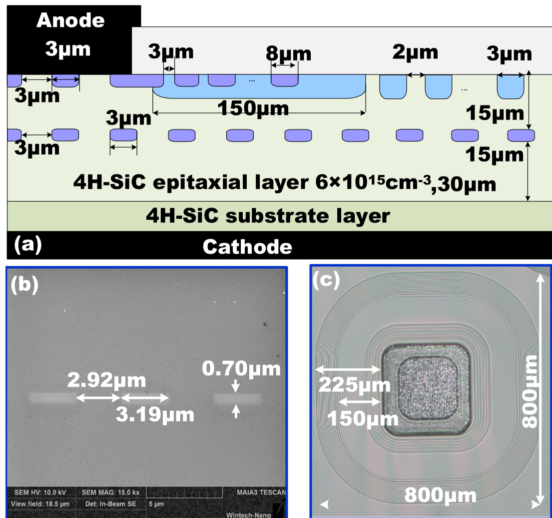

FIGURE 3. (a) Cross-sectional view of the 4H-SiC FJ_JBS diode, (b) SEM image of the FJ structure, and (c) top view of the fabricated FJ device.

TABLE 2. Parameters of the GA-JTE-OR termination structure.

Parameters	*Value*
Length of the JTE	150 μm
Width of the inner rings	8 μm
Spacing of the inner rings	3 μm
Number of the inner rings	5
Width of the outer rings	3 μm
Spacing of the outer rings	2 μm
Number of the outer rings	15

with our FJ_JBS fabrication process, where the GA parts can be fabricated with the main junction in the active region and only one additional implantation process is needed to form the JTE and OR parts [21]–[23]. 2) The GA-JTE-OR can shift the highest peak electric field from the edge of the main junction to the last guard ring. Additionally, both GA and OR structures can relieve the high electric field peak at the edge of the main junction and the main JTE structure by increasing the number of the peak electric field, which can enhance the device reliability [24], [25].

The parameters of the GA-JTE-OR termination structure designed for the *FJ* device are shown in Table 2. The length of the JTE structure is 150 μm. The width and spacing of the inner rings, formed with the main junction, are 8 μm and 3 μm, respectively, which can decrease the sensitivity of *BV* for the low-dose case of the JTE structure [24], [26]. In addition, the width and spacing of the outer rings, formed with the JTE structure, are 3 μm and 2 μm, respectively, which can reduce the sensitivity of *BV* for the high-dose case of the JTE structure [20], [25]. Additionally, 5 inner rings and 15 outer rings are used to effectively shift the field crowding away from the main junction and the edge of the main JTE structure [25], [26].

Figure 4 compares the simulated *BV* values of the single-zone JTE and the optimized GA-JTE-OR, and the breakdown point is set as the current abruptly increases. The GA-JTE-OR

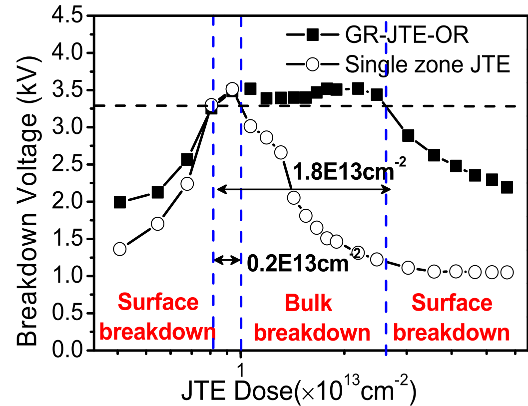

FIGURE 4. *BV* of the FJ device versus the JTE dose for the single-zone JTE and GA-JTE-OR.

shows a better JTE dose tolerance, implying that our selected JTE structure parameters are reasonable. The JTE dose window of the GA-JTE-OR that makes *BV* exceed 3.3 kV is $1.8 \times 10^{13}\text{cm}^{-2}$. For comparison, the single-zone JTE has a narrow window of only $0.2 \times 10^{13}\text{cm}^{-2}$.

To describe the working mechanism of the JTE structure for the *FJ* device, the effect of the JTE dose on *BV* of the *FJ* device that adopts the GA-JTE-OR structure is analyzed. The electric field distributions at the breakdown point with different JTE doses ($6.0 \times 10^{12}\text{cm}^{-2}$, $1.5 \times 10^{13}\text{cm}^{-2}$, and $4.2 \times 10^{13}\text{cm}^{-2}$) are simulated, as shown in Figure 5(a). In addition, the electric field distributions along the surface (AA') and *FJ* location (BB') are shown in Figure 5(b). When the JTE dose is lower or higher than the optimal value, the maximum electric field (E_{max}) occurs at the inner or outer junction termination region, respectively, implying that premature breakdown occurs at the surface. However, if the JTE dose is suitable, E_{max} is notably located at the *FJ* region. In this case, the *FJ* device exhibits bulk breakdown, leading to the surface electric field of the device at the termination region being reduced and uniform and *BV* increases effectively. Meanwhile, it can be observed that the extension of the electric field at the surface is larger than the extension of the electric field at the FJ structure, indicating that the chip area of the FJ device is determined by the termination structure, which is consist with the conventional device. The electric field distributions along the Y-coordinate at the position E_{max} (DD', EE' and FF') are shown in Figure 5(c). The top and bottom epitaxial layers can both withstand the high reverse voltage effectively if E_{max} occurs in the bulk. In addition, there is almost no electric field distribution in the bottom epitaxial layer at E_{max} when the electric field at the surface reaches its critical value. Therefore, it can be inferred that the 4H-SiC *FJ* device will achieve better reverse performance if the breakdown occurs at the bulk region based on a reasonable termination design.

III. DEVICE FABRICATION AND CHARACTERISTICS

The devices were fabricated according to the analysis above. First, the epitaxial layer was grown based on our design.

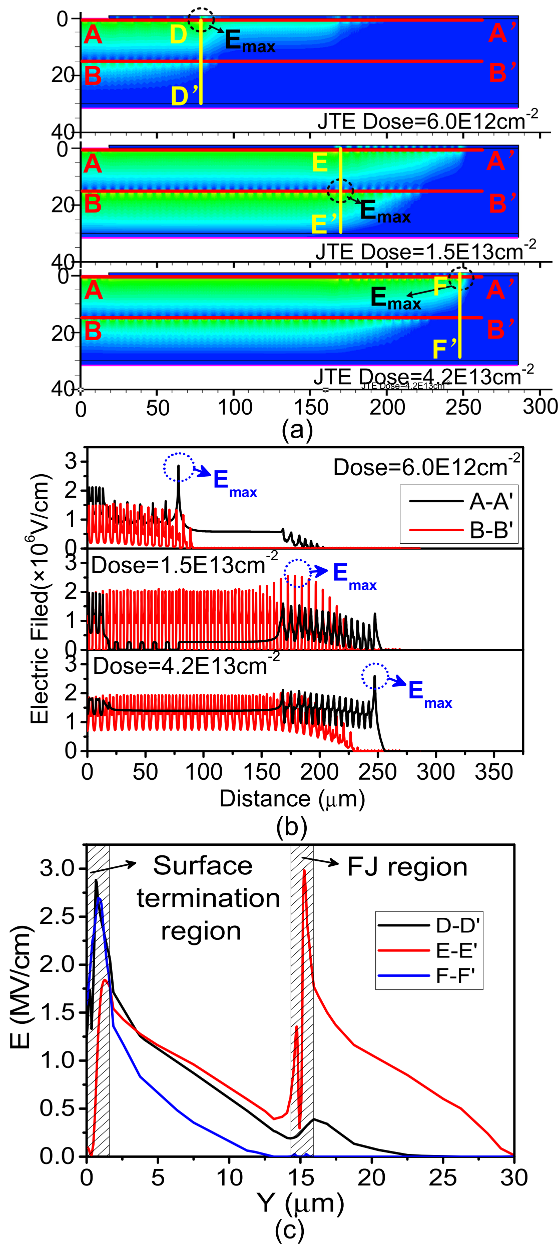

FIGURE 5. (a) Electric field distribution at breakdown for the GA-JTE-OR with different JTE doses, (b) electric field distribution along the surface (AA') and FJ location (BB') at breakdown for the GA-JTE-OR with different JTE doses, and (c) electric field distribution along the Y-coordinate at the position E_{max} (DD', EE' and FF').

After the bottom epitaxial layer grown, the *FJ* structure was formed by selective multiple-energy Al^+ implantation with a box profile on the bottom epitaxial layer, where the total dose was 8×10^{13} cm^{-2}. Figure 3(b) shows the SEM image of the fabricated *FJ* structure in the epitaxial layer, verifying that a box implantation region with a depth of approximately 0.7 μm was achieved, where the width and spacing of the *FJ* structure were both approximately 3 μm. Finally, the top epitaxial layer was grown. The thickness and doping concentration of the bottom and top epitaxial layers were 15 μm and 6×10^{15} cm^{-3}, respectively.

After RCA cleaning, surface passivation was accomplished by thermal oxidation in wet oxygen and a 200nm SiO_2 layer was formed by PECVD process. Then the surface p+ region for the JBS and GA-JTE-OR termination structures were formed using a standard multiple-energy Al^+ implantation fabrication process, where the total dose of the p+ region and JTE are set as 2.5×10^{14} cm^{-2} and 1.5×10^{13} cm^{-2}, respectively. Activation annealing was carried out in Ar at 1650 °C for 40 min. Additionally, the back ohmic metal and top Schottky metal used in our devices were both Ni, where the annealing conditions were 1000 °C for 3 min and 650 °C for 3 min, respectively, in Ar. Finally, a thick polyimide was formed as the last passivation layer. The top view of the fabricated FJ_JBS is shown in Figure 3(c). In addition, the FJ Schottky barrier diode(FJ_SBD) structure and conventional devices were fabricated simultaneously for comparison.

The typical reverse characteristics of the fabricated FJ_JBS and other structures are shown in Figure 6(a). Compared with the *BV* value of 2.55 kV achieved by the conventional JBS, the *BV* value of the fabricated FJ_JBS is as high as 3.4 kV at 100 μA, increasing by approximately 850 V (33.3%) and yielding the highest *BV* value reported for 4H-SiC *FJ* devices. The experimental results demonstrate the advantage of the *FJ* structure for enhancing the device breakdown performance. On the other hand, *BV* of the fabricated FJ_SBD and SBD are 3.53 kV and 2.6 kV, respectively, at 1 mA, confirming that the *FJ* structure plays an important role in improving the device reverse characteristic too. Meanwhile, both the fabricated conventional and FJ devices are measured before and after the wafer is diced. The results indicate that there is no change in the reverse characteristic for the conventional and FJ devices, demonstrating that the reverse performance of the FJ device dose not degrade after scribing.

Figure 6(b) shows the forward characteristics of the fabricated 4H-SiC FJ_JBS and other three structures. The current densities of the *FJ* devices are slightly lower than that of the conventional devices due to the *FJ* structure embedding the epitaxial layer. The differential values of $R_{\text{on,sp}}$ are measured to be 5.67 mΩ·cm^2, 5.34 mΩ·cm^2, 5.20 mΩ·cm^2 and 5.13 mΩ·cm^2 for FJ_JBS, FJ_SBD, conventional JBS and SBD, respectively. The simulated I-V relation of the FJ_JBS is also shown in Figure 6(b). Good agreement between the simulated and experimental results is indicated, proving that the selected parameters in the simulations are reasonable.

The mean curves and error bars of *BV* and R_{on-sp} for the fabricated devices are shown in Figure 6(c), and more than 30 diodes are measured for each type. The four types of fabricated devices maintain stable forward and reverse performance. Furthermore, the experimental results verify our design and confirm the reasonableness of the selected parameters.

Figure 7(a) shows the tradeoff between *BV* and $R_{\text{on}-\text{sp}}$ for our fabricated devices and some other reported results. Our FJ_JBS successfully breaks the theoretical 1-D limit of a unipolar-SiC device (considering a substrate resistance of 0.6 mΩ·cm^2), which is uniquely determined by the material

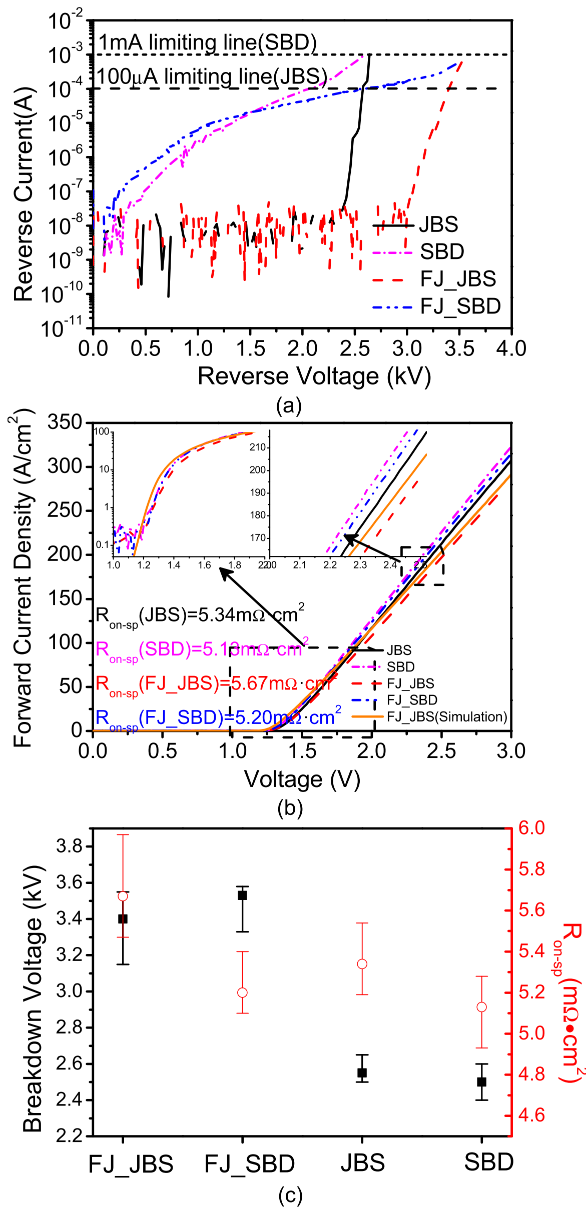

FIGURE 6. **(a) Typical reverse characteristics of the four types of fabricated devices, (b) typical forward characteristics, (c) mean curves and error bars of BV and R_{on-sp}.**

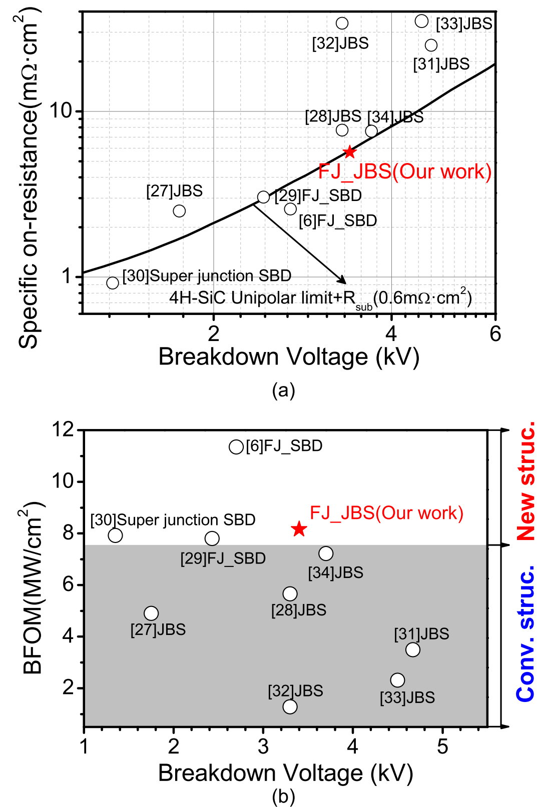

FIGURE 7. **(a) Tradeoff between BV and R_{on-sp} of the fabricated devices and other reported devices, and (b) BFOM value of the fabricated devices and other reported devices.**

properties($R_{on-sp} = 4BV^2/\varepsilon_s\mu_n E_c^3$), showing that the 1-D limit of a unipolar-SiC devices can be experimentally broken by the new *FJ* device structure [35].

Figure 7(b) presents the calculated BFOM values (BFOM=$4BV^2/R_{on-sp}$) of the fabricated JBS. The FJ-JBS achieves a BFOM value of 8.16 GW/cm^2 in this paper, which is lower than that in Ref. [6,7]. Moreover, the fabricated *FJ* devices exhibit performance superior to conventional devices, in agreement with our analysis, proving that *FJ* structure can effectively improve the device electrical performance.

Finally, as shown in Figure 2(c), thanks to a *FJ* device which adopts a relatively high doping concentration (exceeding 6×10^{15}cm^{-3} and closing to 7.5×10^{15}cm^{-3}) for the epitaxial layer can achieve a *BV* value nearly equal to that available with 6×10^{15}cm^{-3} at a lower R_{on-sp}, it can be inferred that the *FJ* device might exhibit better tradeoff in the future if a slightly higher doping concentration of the epitaxial layer is selected and precisely controlled. Moreover, the switch characteristic of the FJ device is also important, the switch characteristic and corresponding device performance will be evaluated in the future.

IV. CONCLUSION

In this paper, we introduce a newly fabricated high-performance 4H-SiC FJ_JBS diode based on a designed epitaxial layer with a thickness of 30 μm, a doping concentration of 6×10^{15}cm^{-3}, and the *FJ* structure is located in the middle of the epi-layer. The *BV* value of the fabricated FJ_JBS is 3.4 kV, yielding the highest *BV* value reported for 4H-SiC *FJ* diodes. In contrast, the conventional JBS, whose epitaxial layer is grown twice (15 μm plus another 15 μm), fabricated on the same wafer achieves a *BV* value of only 2.55 kV, implying that the *FJ* structure plays an important role in increasing the device reverse performance and that our design is reasonable. The corresponding BFOM of this FJ_JBS diode is 8.16 GW/cm^2.

REFERENCES

[1] A. Salemi, H. Elahipanah, C. M. Zetterling, and M. Östling, "Conductivity modulated and implantation-free 4H-SiC Ultra-High-Voltage PiN diodes," *Mater. Sci. Forum*, vol. 924, pp. 568–572, Jun. 2018.

[2] H. Niwa, J. Suda, and T. Kimoto, "Ultrahigh-voltage SiC MPS diodes with hybrid unipolar/bipolar operation," *IEEE Trans. Electron Devices*, vol. 64, no. 3, pp. 874–881, Mar. 2017.

[3] W. J. Sung, K. J. Han, and B. J. Baliga, "Design and manufacturing of 1200 V SiC JBS diodes with low on-state voltage drop and reverse blocking leakage current," *Mater. Sci. Forum*, vol. 924, pp. 613–616, Jun. 2018.

[4] T. Hatakeyama, J. Nishio, and T. Shinohe, "Process and device simulation of a SiC floating junction Schottky barrier diode (Super-SBD)," *Mater. Sci. Forum*, vols. 483–485, pp. 921–924, May 2005.

[5] T. Hatakeyama, C. Ota, J. Nishio, and T. Shinohe, "Optimization of a SiC super-SBD based on scaling properties of power devices," *Mater. Sci. Forum*, vols. 527–529, pp. 1179–1182, Oct. 2006.

[6] J. Nishio, C. Ota, T. Hatakeyama, T. Shinohe, K. Kojima, S.-I. Nishizawa, and H. Ohashi, "Ultralow-loss SiC floating junction Schottky barrier diodes (super-SBDs)," *IEEE Trans. Electron Devices*, vol. 55, no. 8, pp. 1954–1960, Aug. 2008.

[7] C. Ota, J. Nishio, K. Takao, T. Hatakeyama, T. Shinohe, K. Kojima, S. I. Nishizawa, and H. Ohashi, "Doping concentration optimization for ultra-low-loss 4H-SiC floating junction Schottky barrier diode (super-SBD)," *Mater. Sci. Forum*, vols. 615–617, pp. 655–658, Mar. 2009.

[8] S. Yang, Y. Zhang, Q. Song, X. Tang, Y. Zhang, T. Huo, S. Liu, and H. Yuan, "Influence of three-dimensional p-buried layer pattern on the performance of 4H-SiC floating junction Schottky barrier diode," *Jpn. J. Appl. Phys.*, vol. 54, no. 10, Oct. 2015, Art. no. 100302.

[9] H. Yuan, X. Tang, Q. Song, Y. He, X. He, Y. Zhang, and Y. Zhang, "The analysis and characteristics of 4H-SiC floating junction JBS diodes with different structures underneath the termination region," *Solid-State Electron.*, vol. 160, Oct. 2019, Art. no. 107620.

[10] H. Yuan, X. Tang, Q. Song, Y. Zhang, Y. Zhang, F. Yang, and Y. Niu, "Analytical models of on-resistance and breakdown voltage for 4H-SiC floating junction Schottky barrier diodes," *Solid-State Electron.*, vol. 103, pp. 83–89, Jan. 2015.

[11] G. Pensl, "SiC material properties," *Int. J. High Speed Electron. Syst.*, vol. 15, no. 4, pp. 705–745, Dec. 2005.

[12] S. M. Sze, *Physics of Semiconductor Devices*. New York, NY, USA: Wiley, 1981.

[13] A. Galeckas, J. Linnros, V. Grivickas, U. Lindefelt, and C. Hallin, "Auger recombination in 4H-SiC: Unusual temperature behavior," *Appl. Phys. Lett.*, vol. 71, no. 22, pp. 3269–3271, Dec. 1997.

[14] N. T. Son, W. M. Chen, O. Kordina, A. O. Konstantinov, B. Monemar, E. Janzen, D. M. Hnfman, D. Volm, M. Drechsler., R. K. Mever, "Electron effective masses in 4H SiC," *Appl. Phys. Lett.*, vol. 66, no. 9, pp. 1074–1076, 1995.

[15] M. Ruff, H. Mitlehner, and R. Helbig, "SiC devices: Physics and numerical simulation," *IEEE Trans. Electron Devices*, vol. 41, no. 6, pp. 1040–1054, Jun. 1994.

[16] P. T. Landsberg and G. S. Kousik, "The connection between carrier lifetime and doping density in nondegenerate semiconductors," *J. Appl. Phys.*, vol. 56, no. 6, pp. 1696–1700, Sep. 1984.

[17] P. Losee, "Design, fabrication and characterization of high voltage 4H-SiC junction rectifiers for power switching application," Ph.D. dissertation, Rensselaer Polytech. Inst., Troy, NY, USA, 2007.

[18] A. O. Konstantinov, Q. Wahab, N. Nordell, and U. Lindefelt, "Ionization rates and critical fields in 4h silicon carbide," *Appl. Phys. Lett.*, vol. 71, no. 1, pp. 90–92, 1997.

[19] R. Raghunathan and B. J. Baliga, "Temperature dependence of hole impact ionization coefficients in 4H and 6H-SiC," *Solid-State Electron.*, vol. 43, no. 2, pp. 199–211, Feb. 1999.

[20] K. Kinoshita, T. Hatakeyama, O. Takikawa, A. Yahata, and T. Shinohe, "Guard ring assisted RESURF: A new termination structure providing stable and high breakdown voltage for SiC power devices," in *Proc. 14th Int. Symp. Power Semiconductor Devices Ics*, Jun. 2002, pp. 253–256.

[21] A. Mahajan and B. J. Skromme, "Design and optimization of junction termination extension (JTE) for 4H–SiC high voltage Schottky diodes," *Solid-State Electron.*, vol. 49, no. 6, pp. 945–955, Jun. 2005.

[22] Y. Huang, Y. Wang, X. Kuang, W. Wang, J. Tang, and Y. Sun, "Step-double-zone-JTE for SiC devices with increased tolerance to JTE dose and surface charges," *Micromachines*, vol. 9, no. 12, p. 610, 2018.

[23] J.-Y. Jiang, H.-C. Hsu, K.-W. Chu, C.-F. Huang, and F. Zhao, "Experimental study of counter-doped junction termination extension for 4H–SiC power devices," *IEEE Electron Device Lett.*, vol. 36, no. 7, pp. 699–701, Jul. 2015.

[24] R. Perez, D. Tournier, A. Perez-Tomas, P. Godignon, N. Mestres, and J. Millan, "Planar edge termination design and technology considerations for 1.7-kV 4H-SiC PiN diodes," *IEEE Trans. Electron Devices*, vol. 52, no. 10, pp. 2309–2316, Oct. 2005.

[25] L. Yuan, Q. Song, X. Tang, Y. Zhang, L. Guo, Y. Zhang, and Y. Zhang, "Geometrical effects in JTE rings termination for 4H-SiC medium-voltage devices," *Semicond. Sci. Technol.*, vol. 32, no. 12, Dec. 2017, Art. no. 125015.

[26] R. Perez, D. N. Mestres, X. Jorda, P. Godignon, and J. Pascual, "Optimisation of junction termination extension for the development of a 2000 v planar 4H-SiC diode," *Diamond Rel. Mater.*, vol. 12, nos. 3–7, pp. 1231–1235, Mar. 2003.

[27] N. Ren and K. Sheng, "2.5 mΩ.cm^2, 1750 V 4H-SiC junction barrier Schottky diodes with floating guard ring termination structure," *Proc. CSEE*, vol. 35, no. 21, pp. 5552–5559, 2015.

[28] W. J. Ni, "3300 V-10A SiC Schottky diodes," *Semicond. Devices*, vol. 39, no. 11, pp. 823–825, 2014.

[29] C. Ota, J. Nishio, T. Hatakeyama, T. Shinohe, K. Kojima, S. Nishizawa, and H. Ohashi, "Fabrication of 4H-SiC floating junction Schottky barrier diodes(super-SBDs) and their electrical properties)," *Mater. Sci. Forum*, vols. 527–529, pp. 1175–1178, Oct. 2006.

[30] X. Zhong, B. Wang, J. Wang, and K. Sheng, "Experimental demonstration and analysis of a 1.35-kV 0.92-m $\Omega.cm^2$ SiC superjunction Schottky diode," *IEEE Trans. Electron Devices*, vol. 65, no. 4, pp. 1458–1465, Apr. 2018.

[31] J. Schoeck, J. Buettner, M. Rommel, T. Erlbacher, and A. J. Bauer, "4.5 kV SiC junction barrier Schottky diodes with low leakage current and high forward current density," *Mater. Sci. Forum*, vol. 897, pp. 427–430, May 2017.

[32] P. A. Ivanov, I. V. Grekhov, N. D. Il'inskaya, O. I. Kon'kov, A. S. Potapov, T. P. Samsonova, and O. U. Serebrennikova, "High-voltage (3.3 kV) 4H-SiC JBS diodes," *Semiconductors*, vol. 45, no. 5, pp. 668–672, May 2011.

[33] Y. H. Tao, R. H. Huang, G. Chen, S. Bai, and Y. Li, "4.5kV SiC JBS diodes," *Appl. Mech. Mater.*, vols. 347–350, pp. 1506–1509, Aug. 2013.

[34] H. Yuan, Q. Song, X. Tang, Y. Zhang, Y. Zhang, and Y. Zhang, "Design and experiment of 4H-SiC JBS diodes achieving a near-theoretical breakdown voltage with non-uniform floating limiting rings terminal," *Solid-State Electron.*, vol. 123, pp. 58–62, Sep. 2016.

[35] Q.-W. Song, X.-Y. Tang, H. Yuan, Y.-H. Wang, Y.-M. Zhang, H. Guo, R.-X. Jia, H.-L. Lv, Y.-M. Zhang, and Y.-M. Zhang, "Fabrications and characterizations of high performance 1.2 kV, 3.3 kV, and 5.0 kV class 4H–SiC power SBDs," *Chin. Phys. B*, vol. 25, no. 4, Apr. 2016, Art. no. 047102.

HAO YUAN received the Ph.D. degree in microelectronics and solid-state electronics from Xidian University, Xi'an, China, in 2017. He is currently with Xidian University working on the design, fabrication and reliability of SiC power devices.

CHENGSEN WANG was born in Shandong, China, in 1961. He received the B.A. degree in semiconductor physics and devices from the Shandong Engineering College, Shangdong, China, in 1982. He is currently the Chief Engineer and the Deputy General Manager of Jiangsu Jie Jie Microelectronics Company, Ltd., and the General Manager of Jie Jie Semiconductor Company, Ltd. He has been involved in the research and development of semiconductor devices for more than 30 years.

XIAOYAN TANG was born in Xi'an, China, in 1975. She received the M.E. and Ph.D. degrees in microelectronics engineering from Xidian University, Xi'an, in 2002 and 2008, respectively. She is currently a Professor with the School of Microelectronics, Xidian University working on SiC material and devices.

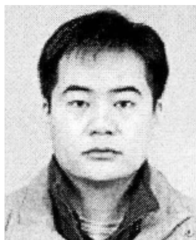

QINGWEN SONG was born in Linshu, China, in 1983. He received the B.A. degree in microelectronics and the M.S. and Ph.D. degrees in microelectronics and solid-state electronics from Xidian University, Xi'an, China, in 2007, 2010, and 2012, respectively. He is currently a Professor with the School of Microelectronics, Xidian University working on modeling and design of SiC power devices.

YANJING HE received the Ph.D. degree in microelectronics and solid-state electronics from Xidian University, Xi'an, China, in 2018. She is currently with Xidian University working on the design, fabrication and reliability of SiC power devices.

YIMEN ZHANG (Senior Member, IEEE) has been a Visiting Scholar with Arizona State University, Tempe, AZ, USA, and a Senior Visiting Scholar with Yale University, New Haven, CT, USA. He is currently a Professor with the School of Microelectronics, Xidian University, Xi'an, China. His current research interests include wideband semiconductor devices, semiconductor devices modeling, TCAD for VLSI, and quantum well devices.

YUMING ZHANG (Senior Member, IEEE) received the M.S. degree from Xidian University, Xi'an, China, in 1992, and the Ph.D. degree from Xi'an Jiaotong University, Xi'an, in 1998.

Since 2001, he has been a Professor with the Microelectronics Institute, Xidian University. His current research interests include design, modeling, fabrication, and electrical characterization of SiC electronic devices for high-temperature and high-power operation.

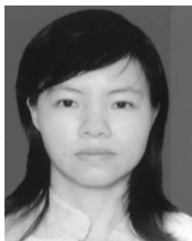

LI XIAO was born in Guang'an, Sichuan, China, in 1976. She received the B.A. degree in microelectronics technology from the Xi'an University of Technology, Xi'an, China, in 2000. Since 2012, she has been working with ZTE Corporation and in charge of component management and research.

LIANGYONG WANG was born in Shengzhou, Zhejiang, China, in 1979. He received the B.A. degree in communication engineering and the M.S. degree in microelectronics from Xidian University, Xi'an, China, in 2002 and 2006, respectively. After graduation, he has been working in ZTE Corporation and in charge of material management and research.

YONG WU was born in Harbin, China, in 1976. He received the M.E. degree in materials science and engineering from Xidian University, Xi'an, China, in 2006. He is currently an Associate Professor with the Xidian-Wuhu Research Institute working on automotive electronics and integrated circuit specialty.